

- Is it “de-disperse” or “de-disperse?” let’s make sure
↳ pick one throughout...
- We need to differentiate between “bursts” & “sub-bursts” throughout.

Evidence of a shared spectro-temporal law between sources of repeating fast radio bursts

Mohammed A. Chamma,^{1*} Fereshteh Rajabi,^{2,3} Christopher M. Wyenberg,¹
Abhilash Mathews⁴ and Martin Houde^{1†}

¹Department of Physics and Astronomy, The University of Western Ontario, 1151 Richmond Street, London, Ontario N6A 3K7, Canada

²Perimeter Institute for Theoretical Physics, Waterloo, ON N2L 2Y5, Canada

³Institute for Quantum Computing and Department of Physics and Astronomy, The University of Waterloo, 200 University Ave. West, Waterloo, Ontario N2L 3G1, Canada

⁴Plasma Science and Fusion Center, Massachusetts Institute of Technology, 77 Massachusetts Avenue, Cambridge, MA 02139, USA

ABSTRACT

We study the spectro-temporal characteristics of two repeating fast radio bursts (FRBs), namely, FRB 180916.J0158+65 and FRB 180814.J0422+73, and combine the results with those from our earlier analysis on FRB 121102. The relationship between the frequency drift rate of individual sub-bursts and their temporal duration is investigated. *We consider a generous broad range of possible dispersion measure (DM) values for each source to understand the range of valid sub-burst drift rate and duration measurements for each burst and to constrain our results. Within these constraints we find good agreement with an inverse scaling law between the two parameters previously predicted using a simple dynamical relativistic model for all sources.* The remarkably similar behavior observed in all sources provides strong evidence that a single and common underlying physical phenomenon is responsible for the emission of signals from these three FRBs, despite their associations with different types of host galaxies at various redshifts. It also opens up the possibility that this sub-burst drift law may be a universal property among repeating FRBs, or at least for a significant subclass among them.

Key words: radiation: dynamics – relativistic processes – radiation mechanisms: non-thermal

1 INTRODUCTION

Fast radio bursts are short duration (\sim millisecond) bursts of energy at radio wavelengths exhibiting large brightness temperatures ($T_B > 10^{32}$ K; Lorimer et al. 2007; Petroff et al. 2019), indicating that these signals originate from non-thermal objects through some coherent emission mechanism. Still, the origin and underlying physical mechanism of FRBs remain unknown in spite of the large number of proposed models. FRB signals also undergo a high level of dispersion as they propagate from the source to the observer, a phenomenon quantified through the dispersion measure (DM). This dispersion results from the wavelength dependence of the refractive index of ionized matter in astronomical media through which radiation travels at varying speeds as a function of frequency. While a first Galactic FRB was recently reported by the CHIME/FRB Collaboration and the STARE2 team toward the Galactic magnetar SGR 1935+2154 (The CHIME/FRB Collaboration et al. 2020; Bochenek et al. 2020), the DM values measured for most FRBs suggest that these signals must emanate from extragalactic sources.

Reported FRBs fall into two groups: one-off events and repeaters. While one-off events form the majority of detections, most of our knowledge about FRBs is based on the study of repeaters. At the time of writing, two repeaters (FRB 121102 and FRB 180916.J0158+65) show periodic behaviours, prompting continued follow-up observations (CHIME/FRB et al. 2020; Rajwade et al. 2020). Importantly, the study of dynamic spectra of repeaters reveals interesting patterns. Among these are a downward drift in the central frequency of consecutive sub-bursts with increasing arrival time within an event (the so-called “sad trombone” effect), and a reduction in the temporal duration of individual sub-bursts with increasing frequency (Gajjar et al. 2018; Hessels et al. 2019; CHIME/FRB et al. 2019; Josephy et al. 2019).

Several models have been proposed to explain these spectro-temporal characteristics. Some models link these characteristics to the intrinsic radiation mechanism of FRBs (Wang et al. 2019; Beloborodov 2020; Metzger et al. 2019) or propagation effects (e.g., plasma lensing (Cordes et al. 2017) or scintillation (Simard & Ravi 2020)), while others argue that a combination of both factors can play a part (Hessels et al. 2019). Recently, the detection of the first Galactic FRB (The CHIME/FRB Collaboration et al. 2020; Bochenek et al. 2020; Kirsten et al. 2020) has posed new chal-

* E-mail: mchamma@uwo.ca
† E-mail: mhoude2@uwo.ca

lenges for existing theoretical models. For example, one sequence of sub-bursts detected toward this source reveals an upward central frequency drift with increasing arrival time (a “happy trombone” effect). A few models have anticipated such a possibility for the spectra of FRBs (Simard & Ravi 2020; Rajabi et al. 2020; Beniamini & Kumar 2020). In particular, in Rajabi et al. (2020) we proposed a simple dynamical relativistic model where a descending or an ascending central frequency drift for a sequence of sub-bursts can be explained based on the intrinsic properties of the corresponding FRB source (as discussed in Section 3.3 and Appendix B). But more importantly, our model also predicts that a steeper frequency drift should be present within individual sub-bursts (henceforth the sub-burst drift) where the slope of the FRB signal as displayed in a dynamical spectrum (i.e., frequency vs. time) obeys a simple law scaling inversely with the temporal duration of the sub-burst. We further provided evidence for this sub-burst drift behavior for FRB 121102 and showed that data taken over a wide range of frequencies for this repeater follows the same law, i.e., the aforementioned inverse scaling of the sub-bursts drift with their corresponding temporal duration. We then argued that this finding implies that the underlying physical process responsible for the signals detected in FRB 121102 is intrinsically narrow-band in nature, while relativistic motions within the source are required to explain the wide observed bandwidths. In this paper, we examine data from two additional repeaters, FRB 180814.J0422+73 (CHIME/FRB et al. 2019) and FRB 180916.J0158+65 (CHIME/FRB Collaboration et al. 2019; CHIME/FRB et al. 2020), and show that this form of law is closely shared between these three FRBs originating from host galaxies at different redshifts. We also consider the effect of the chosen DM on the measurements of the sub-burst drift rate and the burst duration in order to understand the robustness of this relationship between the sources. This significant finding reveals new insights on the underlying physical mechanism at the source of FRB signals and helps refine modelling efforts.

1.1 Triggered Dynamical Model

In Rajabi et al. (2020) we introduced a simple dynamical model where a triggering source (e.g., a pulsar or magnetar; see Houde et al. 2019) is located directly behind an FRB source as seen by an observer. The regions from which FRB signals are emanating are assumed to be moving towards (or away from) the observer, potentially at relativistic speeds. Such a scenario is appropriate for situations where the emitted signal is highly collimated, such as is the case for a radiation process based on Dicke’s superradiance which our proposed FRB model is ultimately inspired by (Rajabi & Houde 2016a,b; Rajabi & Houde 2017; Mathews 2017; Houde et al. 2018; Houde et al. 2019; Rajabi et al. 2019; Rajabi & Houde 2020). Under such conditions we showed that the sub-burst drift from a single FRB signal (for repeaters an event can contain several sub-bursts) obeys the following relation

$$\frac{1}{v_{\text{obs}}} \frac{dv_{\text{obs}}}{dt_D} = -\frac{A}{t_w}, \quad (1)$$

where v_{obs} , t_w and t_D are the frequency, the temporal duration of the FRB sub-burst and the delay before its appearance (in relation to the arrival of the trigger) as measured by the observer. The systemic parameter $A \equiv \tau'_w/\tau'_D$ with τ'_w and τ'_D the corresponding sub-burst proper temporal duration and delay in the FRB reference frame, respectively.

Following the model of Rajabi et al. (2020), the temporal du-

ration of an FRB sub-burst in the observer rest frame is given by

$$t_w = \tau'_w \frac{v_0}{v_{\text{obs}}}, \quad (2)$$

where, as defined earlier, τ'_w , v_0 and v_{obs} respectively are the proper temporal width and frequency of emission in the FRB rest frame, and the frequency of the signal as measured by the observer. Equation (2) clearly predicts an inverse relationship between the observed FRB temporal width and frequency, which had previously been noticed and studied. For example, a verification of this effect can be found in Figure 7(b) of Gajjar et al. (2018) for the case of FRB 121102. Although the burst temporal duration exhibits a fair amount of scattering at a given frequency (inherent to τ'_w in equation (2)), the predicted behavior is clearly observed. Since the data used for this source come from observations spanning a wide range of frequencies, it further follows from equation (2) that the rest frame frequency v_0 cannot change significantly as a function of v_{obs} , as this would affect the inverse relationship observed in the data.

Rajabi et al. (2020) also derived the following equation for the drift in the observed central frequency of a sequence of sub-bursts with increasing arrival time

$$\frac{\Delta v_{\text{obs}}}{\Delta t_D} = \frac{v_{\text{obs}}}{v_0} \frac{dv_{\text{obs}}}{d\tau'_D}, \quad (3)$$

where the term on the left-hand side is for the central frequency drift and τ'_D is the proper temporal delay between the arrival of the trigger and the emission of the ensuing sub-burst in the FRB rest frame. The derivative $dv_{\text{obs}}/d\tau'_D$ is a physical parameter characterizing the environment of the FRB source, which determines whether the sequence of sub-bursts has the appearance of a “sad” ($dv_{\text{obs}}/d\tau'_D < 0$) or “happy trombone” ($dv_{\text{obs}}/d\tau'_D > 0$; see Rajabi et al. 2020 for more details). Equation (3) predicts that the central frequency drift should scale linearly with v_{obs} , which has previously been verified for FRB 121102 over a wide range of frequencies. This can be asserted, for example, from Figure 3 (top panels) of Hessels et al. (2019). Once again, this observed dependency could not be realized if v_0 changed significantly in equation (3).

2 BURST ANALYSIS

Although equation (1) was tested and verified for FRB 121102 in Rajabi et al. (2020) using previously published data covering more than a decade in frequency (Michilli et al. 2018; Gajjar et al. 2018; Josephy et al. 2019), it was not known at the time whether it applies equally well to other repeating FRBs. We therefore retrieved and analyzed previously published data for two other sources discovered by the CHIME/FRB Collaboration (Fonseca et al. 2020), namely FRB 180916.J0158+65 (CHIME/FRB et al. 2020) and FRB 180814.J0422+73 (CHIME/FRB et al. 2019). These data are all contained within the CHIME/FRB spectral band (approximately 400–800 MHz) and the corresponding dynamic spectra were analyzed using the two-dimensional autocorrelation technique introduced in Hessels et al. (2019), resulting in estimates for the sub-burst drift (dv_{obs}/dt_D) and temporal duration (t_w). See Appendix A for more details. These data sources were chosen purely due to their ease of accessibility and the support available, and other sources are not included due to difficulties in accessing and handling. Ultimately we aim to extend this analysis to as many sources as possible.

Source	Data	DM Range (pc/cm ³)
FRB121102	Michilli et al. 2018	554.1-565.3
FRB121102	Gajjar et al. 2018	555-570 (555-583)
FRB180916.J0158+65	CHIME/FRB et al. 2020	346.82-349.82
FRB180814.J0422+73	CHIME/FRB et al. 2019	188.7-190.0

Table 1. The range of DMs used to determine the range of possible values of each burst's sub-drift rate and duration. These are chosen to be as wide as possible while still obtaining reasonable sub-drift rate measurements based on the uncertainties. In general, the range of DMs observed burst-to-burst determines the range used, with some DMs on the higher end excluded due to positive drift rates and distortion observed when dedispersing to those DMs. The DM range in parentheses is used specially for burst 11D from Gajjar et al. 2018 due to its high S/N optimized DM. See the text for more details.

2.1 Effect of Dispersion Measure (DM)

Since the measurement of any drift rate (or almost any other spectro-temporal feature) is strongly dependant on the DM that is used to dedisperse a dynamic spectrum, and since the DM of a source can potentially vary from burst to burst as well as with time, we studied the variation of our drift and duration measurements for each burst at different choices of DM. Dedispersion can be performed by optimizing either the signal-to-noise (S/N) or a structure parameter and can result in very different values found for the DM depending on the burst (e.g. Fig 1 of Gajjar et al. 2018). In particular, an algorithm seeking to choose a DM by maximizing S/N might stack the components of a complex bursts and yield a DM value that is higher than a structure optimizing algorithm. For bursts with components that are not clearly resolved it becomes ambiguous which algorithm is most accurate and the precision in the DMs determined burst to burst can be much narrower than the variations in the DM observed overall for a source (CHIME/FRB et al. 2020). It therefore becomes difficult to uncouple FRB characteristics from the nature of the medium in order to study relationships between spectro-temporal features as we hope to do. One option is to use the DM found on a burst by burst basis. However, doing this can become a complicated process of verifying that the DM algorithm choice is appropriate, which will often be ambiguous for smeared bursts where it is not clear if it consists of multiple components or not. Without a detailed understanding of the emission mechanism, the medium, the source, and the resulting DM distribution as a function of time, it is in fact much simpler and more conservative to choose a DM range as wide as possible based on the history of DMs found for the source. We shall see that despite the significant uncertainties this choice entails, the data still point to the existence of an inverse trend between the sub-burst drift and the burst duration for the three sources considered here.

Table 1 shows the DM ranges chosen for each source and dataset, in each case aiming to consider as broad a range of DMs as possible while still obtaining reasonable sub-drift rate measurements. For the data used from Michilli et al. 2018 dispersion measure variations are believed by those authors to be $\lesssim 1\%$ of 559.7 pc/cm³, and therefore consider a range of 554.1-565.3 pc/cm³. For the data from Gajjar et al. 2018, due to availability, we use the sub-bursts in burst 11A and burst 11D. A structure optimized DM for 11A is found at 565 pc/cm³, and their Figure 1 indicates that DMs between 555-570 are also close to optimal, so we adopt this range,

For burst 11D, due to a lack of structure we adopt a range of 555-583 to be closer to its S/N optimized DM, however higher DMs are excluded as the drift rates start to become positive (which are not physical according to our model and in general usually indicate too aggressive of a de-dispersion). For data from CHIME/FRB et al. 2020 on FRB 180916.J0158+65 a precise DM of 348.82 ± 0.05 pc/cm³ is found for one of the bursts, but burst-to-burst the DM can range from 348.7-350.2. We therefore choose a mid-point of about 348.82 pc/cm³ and adopt a range of 346.82-349.82 pc/cm³. The lower value for the start of the range is to push the limit of acceptable DMs while still obtaining reasonable drift rate measurements. While we stay away from the higher end of the observed range due to the distortion and positive drift rates observed for most of the bursts at that high of a DM. Finally, for data from CHIME/FRB et al. 2019 on FRB 180814.J0422+73, due to the structure present in the bursts, we adopt the full range of structure optimized DMs found (188.9-190 pc/cm³) but expand the lower end and use 188.7-190 pc/cm³. We ignore the higher S/N optimized DMs due to the component stacking and distortion observed when de-dispersing to those DMs.

For each source, we generate a grid of DMs over the DM range chosen and dedisperse each burst to each DM before performing an auto-correlation analysis. The grid spacing varies from $\Delta \text{DM} \approx 0.1\text{-}2 \text{ pc/cm}^3$ depending on the source, yielding approximately 10-20 trial DMs in each case. For bursts with multiple components like burst 11A from Gajjar et al. 2018 for FRB 121102, the components are separated manually by finding valleys in the corresponding time series of the data. When necessary these components are padded with a background sample of the waterfall so that there is a wide enough temporal extent to properly dedisperse the burst. Some bursts are not clearly resolved, but wherever there is indication that the sub-drift suddenly changes mid-burst a manual attempt is made to separate the components.

The autocorrelation analysis (Appendix A) is then performed for each dedispersed waterfall and yields sub-drift rate and temporal duration measurements for each burst at each DM, and we use these data to determine the range of possible values for each measurement. The dynamic spectra of every burst used in this analysis with its autocorrelation are shown in Figures 6 – 10 at the end of the paper, displayed at one of the trial DMs. The range found for each of these measurements is much larger than the parameter uncertainty from the underlying two-dimensional Gaussian fit, indicating that the covariance between the measurements and the DM is larger than with the model parameters. Since the true underlying DM distribution for each source appears to be narrower than the DM range we have used (considering the distribution so far implied by published DMs and knowing that the distribution can change with time), the range of values found this way must be larger than the range implied by the true uncertainties for each measurement. We therefore treat the range of values found by this analysis as upper-limit estimates of the real measurement uncertainties.

2.2 Burst Exclusions and Fitting

With the measurements for each burst at each trial DM found, there remain measurements that are unconstrained and/or non-physical that need to be discarded before fitting. In particular, we discard any positive sub-drift rate measurements following the assumption of our model that these are artificial, and measurements where the value and/or uncertainties approaches infinity as is the case for bursts that become near vertical or circular in their autocorrelation.

Isn't this what the exclusion does?

As discussed further in Section 3.1, circular, ‘blobby’ bursts tend to have a large uncertainty associated with their fit parameters, while vertical but otherwise elliptically shaped autocorrelations suggest that a slightly lower DM might yield more physical measurements.

The result of this exclusion process is that out of a total of 41 bursts analysed, we retain all the measurements made for 28 bursts over the DM ranges specified in Table 1. For the remaining 13 bursts that have had measurements excluded, we automatically limit the DM range further (in every case except one by lowering the maximum trial DM) to keep the drift rate measurement negative. We therefore mark these bursts specially when displayed in Figures 1 and 5 to indicate the higher possibility of an unconstrained measurement for those points. For all but one of the bursts treated this way, the DM range is only slightly restricted to achieve meaningful drift rate measurements and still spans more than half the original range. For one burst from FRB180814, the DM range is limited more aggressively from $188.7 - 190.0 \text{ pc/cm}^3$ to $188.8 - 188.9 \text{ pc/cm}^3$.

Using this set of drift rate and temporal duration measurements we find a fit to equation (1) at each DM for each source. Each fit is found by using the set of burst measurements found at a particular DM. This fitting procedure yields a range of possible fits over the possible DM range for each source, and allows us to compare agreement between sources. For each fit of equation (1) found we compute the reduced χ^2 and use it to select a representative DM for each source, that is, the DM at which the fit has a reduced χ^2 closest to unity. This representative DM is primarily used for visual purposes, since using a single DM for all the bursts from a source is an approximation. The representative DMs found for each source in this way are 558.8 and 568.3 pc/cm^3 for the data from Michilli et al. 2018 and Gajjar et al. 2018, respectively, and 348.82, and 188.8 pc/cm^3 for FRB180916.J0158+65 and FRB180814.J0422+73. They are shown explicitly in Figure 1.

3 RESULTS AND DISCUSSION

We show in Figure 1 the results of our analysis, where the sub-burst drift rate (normalized to the frequency of observation v_{obs}) is plotted against the temporal width t_w for the three FRBs. Normalizing the sub-burst drift has the advantage of allowing us to combine the different sources on the same graph irrespective of the frequency of observation, shifts due to the dynamical Doppler effect or cosmological redshift. Furthermore, we note that equation (1) is also insensitive to temporal scaling transformations. For example, interstellar scintillation, which brings a temporal broadening scaling inversely with the fourth power of the frequency, will have no effect on our analysis. The only consequence being a shift of data points along the specific law characterized by the parameter A in equation (1). The points displayed in Figure 1 are the measurements of each burst obtained at the optimal DM described at the end of Section 2.2, and the capped lines represent the range of possible measurements for that burst over the DM range considered.

Examination of Figure 1 reveals that the inverse relationship between the two parameters is clearly seen for all sources on the graph for values ranging over two orders of magnitude for both the normalized sub-burst drift rate and the temporal duration. Also shown in the figure are fits for the predicted function A/t_w (see equation (1)) for the three sources at their representative DMs (see end of Section 2.2), with $A = 0.078 \pm 0.006$, 0.082 ± 0.006 and 0.076 ± 0.013 for FRB 121102, FRB 180916.J0158+65 and FRB 180814.J0422+73, respectively. These fits suggest the three

are also non-physical within our model and

sources obey the same scaling of equation (1). The shaded regions for each source represent the range of fits found when considering all DMs in the possible range, and any fit in that range is possible. The range of possible fit parameters are found to be $A = 0.042 - 0.355$, for FRB 121102, $A = 0.030 - 0.153$ for FRB 180916.J0158+65, and $A = 0.071 - 0.152$ for FRB 180814.J0422+73. These regions overlap significantly, but indicate the possibility of unique and distinct fits between the three sources. We note that the range for FRB 180814.J0422+73 is completely contained in either of the other two ranges.

A few important consequences are to be noted from the results presented in Figure 1. First, we consider the possible conclusion that not only is the inverse relationship between the sub-burst drift and duration verified for the three sources, but they do so with similar values for A in equation (1). The different fits to this systemic parameter are similar given their uncertainties, and it is difficult to visually distinguish between the corresponding curves. This closeness between the values obtained for A is rather remarkable and suggests the existence of a single and common underlying physical phenomenon responsible for the emission of FRB signals in the three sources. This is significant because these FRBs are associated with different types of host galaxies at various redshifts. More precisely, FRB 121102 is localized to a low-metallicity irregular dwarf galaxy at a redshift $z = 0.193$ (Tendulkar et al. 2017), while the redshift of FRB 180814.J0422+73 is estimated to be $z \leq 0.1$ (CHIME/FRB et al. 2019). Furthermore, the candidates for the host galaxy of FRB 180814.J0422+73 are not consistent with those harboring long gamma-ray bursts (LGRBs) or superluminous supernovae (SLSNe), unlike the host galaxy of FRB 121102 (Li et al. 2019). As for FRB 180916.J0158+65, it is precisely localized to a star-forming region in a massive spiral galaxy at a redshift $z = 0.037$ (Marcote et al. 2020). This source is the closest known extragalactic FRB, whose host galaxy does not show signatures of a strong magnetic field nor a radio counterpart as reported for FRB 121102.

Besides the possible conclusion that the three sources obey the same law, there are other related inferences that can be made given these results and in light of the difficulty in constraining the measurements of the burst properties. Even with the ranges of measurements seen, Figure 1 strongly suggests each source obeys a form of equation (1), where we see a clear decrease in the magnitude of drift rates with increasing burst duration. We interpret the large overlap between the possible fit regions as an indication that it is likely that these sources obey the same type of law, but that distinct parameters for each source are possible. Several of the bursts from FRB180814.J0422+73 lie close to but outside their region of possible fits and the narrow DM range required to constrain burst measurements for this source may be due to the small bandwidths observed for the bursts available, which increases the uncertainty associated with the sub-drift rate measurement.

As was discussed in Rajabi et al. (2020), the three predictions made by our simple dynamical model (i.e., the narrowing of sub-bursts width t_w with increasing frequency v_{obs} , the sad or happy trombone effect and the sub-burst drift law discussed here) provide strong evidence that the underlying physical phenomenon is narrow-band in nature. This is because the dependencies on v_{obs} and the frequency of emission in the FRB rest frames v_0 for the three predicted relationships are such that it would be difficult to envision how they could be realized through the data if v_0 was allowed to vary substantially (see Section 3.3 for more details). Although data over

This is discussed in details in the next paragraph.

First, importantly, the inverse relationship between the sub-burst drift & temporal width is deserved to not be an artefact due to the selection of a given DM. That is, there is an unmistakable tendency for

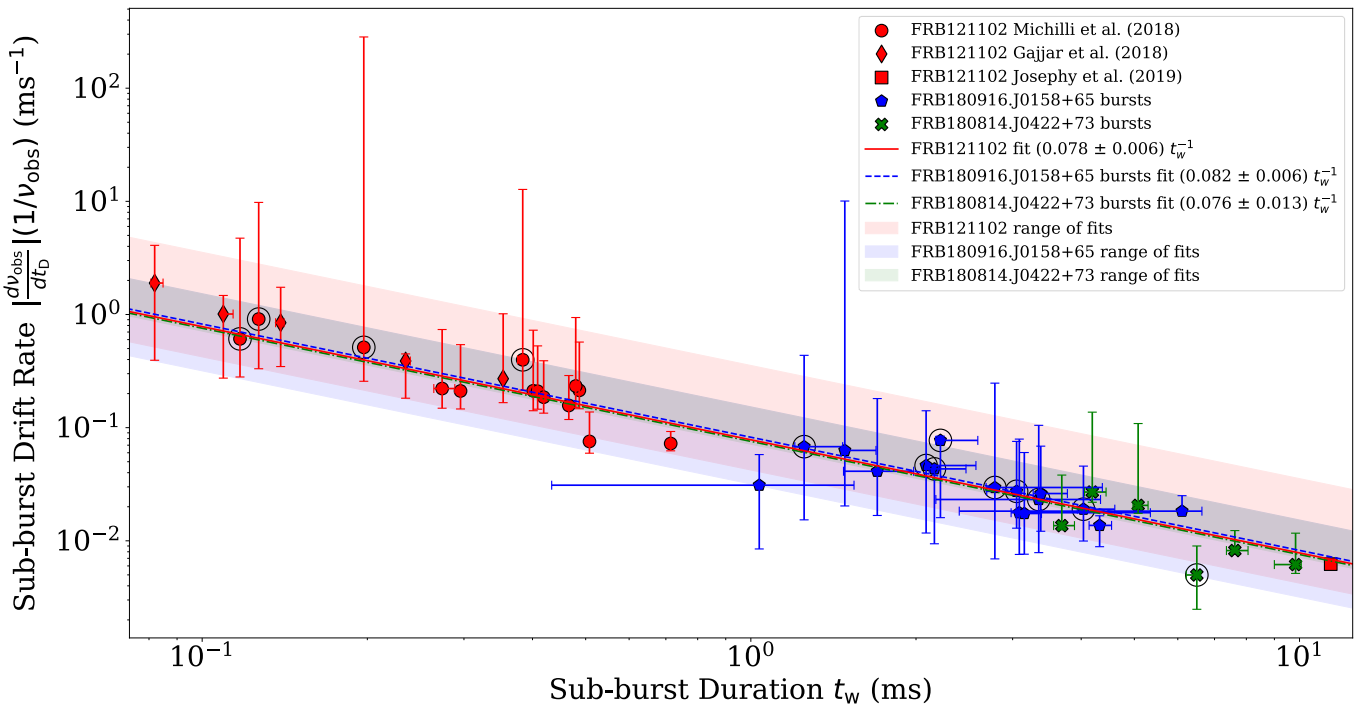


Figure 1. A plot of $|d\nu_{\text{obs}}/dt_0| (1/\nu_{\text{obs}})$ vs. t_0 for bursts from FRB 121102 (red circles, diamonds and square; Gajjar et al. 2018; Michilli et al. 2018; Josephy et al. 2019), FRB 180916.J0158+65 (blue pentagons; CHIME/FRB et al. 2020) and FRB 180814.J0422+73 (green crosses; CHIME/FRB et al. 2019). The sub-burst drift $d\nu_{\text{obs}}/dt_0$ and duration t_0 were obtained using the two-dimensional autocorrelation technique of Hessels et al. (2019), while the center frequency ν_{obs} was estimated from the corresponding dynamic spectra. Each burst was dedispersed to a grid of trial DMs over the range specified by Table 1 and the measurements were repeated. The one point from Josephy et al. 2019 was not part of the same analysis and is shown for reference. The red, blue and green lines are for fits of the function A/t_0 on the FRB 121102, FRB 180916.J0158+65 and FRB 180814.J0422+73 data, respectively, at a DM within the range of trial DMs for which the reduced χ^2 of the fit was closest to one, and are difficult to distinguish from one another. All points except for the red square are of measurements made at the same DM used for the fit line. The capped lines at each point represent the range of possible measurements obtained via the autocorrelation analysis for different DMs over the DM ranges chosen. As discussed in Section 2.1, these are used in lieu of the difficult-to-determine true measurement uncertainties but are necessarily larger than the true uncertainties and can be interpreted as a proxy for the measurement uncertainty introduced by DM uncertainty. The circled points indicate the bursts that required a more limited DM range to constrain their measurements (see Section 2.2). The shaded regions represent the range of fits found when using measurements obtained at other DMs in the range, and represents the range of possible fits. These regions overlap significantly, but indicate the possibility of unique and distinct fits between the three sources within the range of possible DMs chosen.

a significant range of observed frequency is currently only available for FRB 121102 (and constitutes the basis of the analysis presented in Rajabi et al. 2020), the fact that FRB 180916.J0158+65 and FRB 180814.J0422+73 follow the same law renders it reasonable to expect that the conclusions reached for FRB 121102 also apply to them.

We can use this information with our model to further characterise the environment of the sources responsible for the detected bursts. Indeed using the extensive data available for FRB 121102 one can estimate, although with limited precision at this point, the maximum Lorentz factor and the rest frame frequency of emission ν_0 . To do so we will assume highly simplified conditions, i.e., that the different FRB reference frames from which the sub-bursts emanate either move towards or away from the observers with the same range of speeds. We will denote by $\beta^+ > 0$ and $\beta^- = -\beta^+$ the maximum velocities (divided by the speed of light) towards and away from the observer, respectively, with corresponding observed frequencies ν_{obs}^\pm . It is then straightforward to show that, under this

N points for a given source (except for the Josephy et al. datum), these are used in lieu of, and are larger than, the difficult-to-determine measurement uncertainties.

$$\beta^+ = \frac{\nu_{\text{obs}}^+ - \nu_{\text{obs}}^-}{\nu_{\text{obs}}^+ + \nu_{\text{obs}}^-} \quad (4)$$

$$\nu_0^2 = \nu_{\text{obs}}^+ \nu_{\text{obs}}^- \quad (5)$$

Using $\nu_{\text{obs}}^+ \approx 7.5$ GHz and $\nu_{\text{obs}}^- \approx 630$ MHz we find $\beta^+ \approx 0.9$ and $\nu_0 \approx 2.6$ GHz for FRB 121102 (taking into account its known redshift $z = 0.193$ from Tendulkar et al. 2017; see Section 3.3 for more details). Evidently, the accuracy for these estimates is set and limited by the frequency coverage of the existing data and is likely to change as more detections are acquired. For example, confirming the purported detection of signals at 111 MHz from Fedorova & Rodin (2019) would further increase β^+ and bring down ν_0 on the order of 1 GHz. At any rate, these results imply that FRB 121102 is potentially very strongly relativistic.

We also know that the spectral width $\Delta\nu_{\text{obs}}$ associated to sub-bursts for FRB 121102 scales as $\Delta\nu_{\text{obs}} \sim 0.16 \nu_{\text{obs}}$ (see Figure 6 in Rajabi et al. 2020 or Figure 5 in Houde et al. 2019). This spectral extent is the result of motions within a given FRB rest frame from where a sub-burst centred at ν_{obs} originates. As discussed in

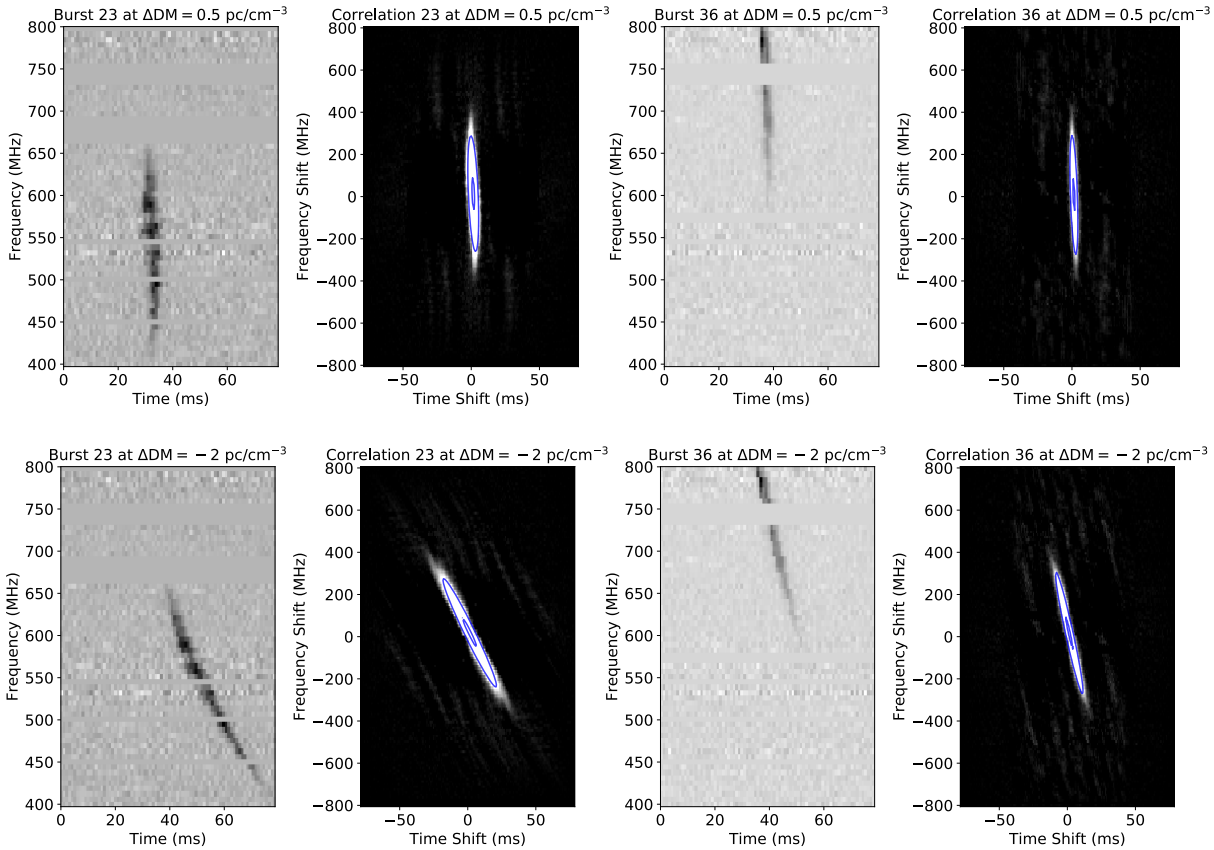


Figure 2. Changes to dynamic spectra and autocorrelation as a function of variations in the DM. Sub-bursts 23 (first column) and 36 (third column) from FRB 180916.J0158+65 are shown with their autocorrelation functions (second and fourth columns, respectively) for two offsets $\Delta\text{DM} = 0.5 \text{ pc cm}^{-3}$ (top row) and -2 pc cm^{-3} (bottom row) from the ‘optimal’ value chosen for our analysis (i.e., $\text{DM} = 348.82 \text{ pc cm}^{-3}$). The rotations brought about by the small changes in DM are clearly seen in both the dynamic spectra and autocorrelation functions.

Appendix B, the observed spectral width is constrained through

$$2\Delta\beta' \leq \frac{\Delta\nu_{\text{obs}}}{\nu_{\text{obs}}} \leq \frac{2\Delta\beta'}{1 - \Delta\beta'^2}, \quad (6)$$

where the motions in the FRB rest frame are contained within $\pm\Delta\beta'$. We thus find $\Delta\beta' \sim 0.08$ with equation (6) for this source.

We thus have a picture where FRB 121102 and similar sources would consist of systems within which a number of spatially distinct FRB rest frames, whose motions cover a wide range of velocities (some highly relativistic relative to the observer), are responsible for the emission of individual sub-bursts. In turn, each such rest frame is also host to mildly relativistic motions, which are responsible for the observed wide spectral widths of sub-bursts.

Finally, we note that our discovery of a shared sub-burst drift law among these three sources suggests that this could be a universal property among repeating FRBs or at least a significant subclass of them. This not only motivates further searches but also provides a new tool to study and categorize FRBs based on their underlying physical mechanism.

In the following sections we discuss the effect of DM variations on the autocorrelation of dynamic spectra as well as the effects of noise on the measurement of the sub-drift rate and the burst duration. We also further discuss the determination of physical parameters of the source.

move to the end of Conclusion.

3.1 DM Variations as a Rotation of the ACT

Based on the study of the variation of measurements over ranges of plausible DMs discussed in 2.1, different DM choices can be seen as rotations of the autocorrelation function of the burst. As an example, we show in Figure 2 two bursts each at two choices of DM. In a given dynamic spectrum, we see that the shape of the burst can appear to ‘distort’ due to the v^{-2} dependence of dispersion, while the shape of the burst’s autocorrelation remains the same while experiencing a rotation. To characterize this further we consider the angle parameter (as opposed to the drift rate derived from said angle) found for the bursts from FRB 180916.J0158+65 against the burst duration derived from the underlying Gaussian fit in Figure 3. This shows that across different DMs the measured duration varies little while the angle found is offset from angles at other DMs by a constant angle. We can demonstrate this using equations (1) and (A2) to find that the drift angle is related to the sub-burst duration through

$$\theta = \arctan \left(\frac{1}{A} \frac{\nu_{\text{res}}}{\nu_{\text{obs}}} \frac{t_w}{t_{\text{res}}} \right), \quad (7)$$

where as before $A \equiv \tau'_w/\tau'_D$. We also approximated ν_{obs} to be constant, which is adequate for this purpose. We find that the chosen fit obtained with equation (7) for the sub-bursts at $\Delta\text{DM} = 0$ (i.e., the solid curve in Figure 3) is also satisfactory for angles corresponding to the different ΔDM values when a simple offset angle (i.e. a rotation) is applied. Similar trends appear to hold for the other

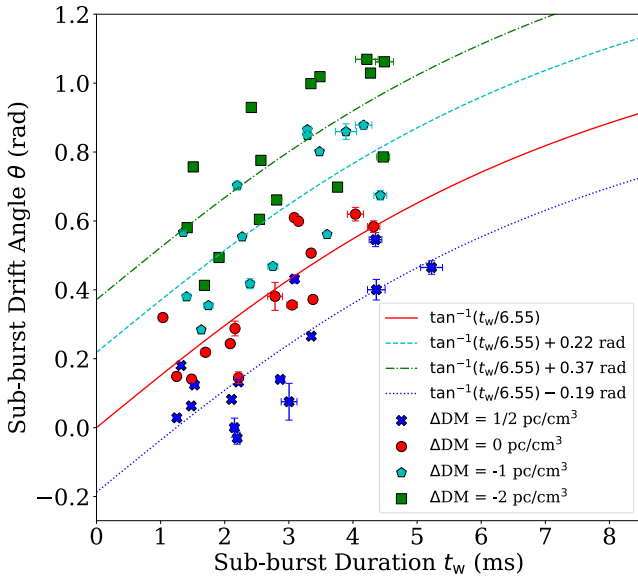


Figure 3. The fit angle θ vs. sub-burst duration t_w from bursts de-dispersed to small variations in the DM for the source FRB 180916.J0158+65. Red circles are sub-bursts at $\Delta\text{DM} = 0$ which corresponds to a $\text{DM} = 348.82 \text{ pc cm}^{-3}$. Blue crosses, cyan pentagons, and green squares are sub-bursts de-dispersed to $\Delta\text{DM} = 0.5, -1$, and -2 pc cm^{-3} , respectively. Error bars indicate the parameter fitting error. The red curve is fit to the red circles and is of the form given in equation (7), derived from the dynamical model described in the main text. Blue, cyan, and green curves are obtained by adding a rotation (i.e., adding an angle) to the $\Delta\text{DM} = 0$ model. As discussed in Section 3.1 this plot demonstrates the rotational effect small variations in the DM can have on the autocorrelation of dynamic spectra of FRBs.

two sources considered, however it is most clear in the example of FRB 180916.J0158+65.

Considering the angle instead of the drift rate during analysis at first appears to avoid the discontinuity in drift rate measurements around $\theta = 0, \pi$, or where the drift rate approaches infinity. If one were not making the assumption that positive drift rates were nonphysical, then the angle might be the measurement of interest. However, since we wish to impose the constraints of negative drift rates as well as a constrained uncertainty on the measurement, a discontinuity near angles that lead to nearly vertical drift rate still exists. The behaviour of drift rate measurements derived from the parameter angle in the context of autocorrelation noise is discussed in more detail in Pleunis (2020) as well as in the dfdt¹ package.

shouldn't that be highlighted?

3.2 Uncertainty due to Frequency Band Masking

As described in Appendix A, we use the 2D autocorrelation technique used in Hessels et al. (2019) to measure the sub-burst drift (dv_{obs}/dt_D) and temporal duration (t_w) via a Gaussian fit optimization procedure. In addition to random signal noise, the dynamic spectra analyzed were complicated by missing frequency bands of data, which would sometimes overlap with the frequency extent of the sub-burst under analysis. In this section we assess the extent of the uncertainty introduced by the missing frequency band data by (1) artificially masking (zero-padding) various trial Gaussian signals of known orientations and characteristic widths, (2) processing them

¹ <https://github.com/zpleunis/dfdt>

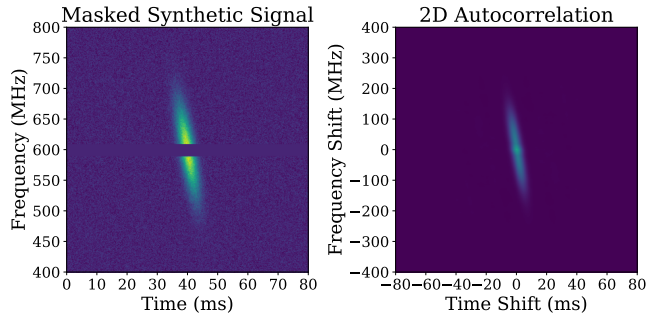


Figure 4. Synthetic Gaussian signal with a masked (zeroed) band (left), and 2D autocorrelation of masked signal (right). The signal shown approximately matches the characteristics of Burst 23 depicted in Figure 8 in each of their temporal widths, their frequency extents, their inclinations, and their total missing frequency bandwidths.

through our pipeline, and (3) comparing the extracted sub-burst drift and duration parameters to the generating parameters.

Consider for example burst 23 of FRB 180916.J0158+65 (CHIME/FRB et al. 2020) pictured, along with its two-dimensional autocorrelation, in Figure 8. Three frequency bands of data are absent from the original data in this burst, and the total missing bandwidth (as a fraction of the frequency extent of the sub-burst) is higher than the fractional bandwidth typically absent from sub-bursts analyzed in the paper. We treat burst 23 as a good example of a waterfall with significant frequency masking.

To estimate the effect of missing frequency channels on our analysis we construct an artificial burst similar to burst 23 from a Gaussian of $a = 67 \text{ MHz}$ (90 pixels), $b = 2.2 \text{ ms}$ (15 pixels), $\theta = 10^\circ$ (inclination from vertical), and with stochastic noise of amplitude 25% that of the Gaussian amplitude. We perform our analysis on a 2D array with dimensions 540×540 pixels, having horizontal and vertical resolutions of 6.75 px/ms and 1.35 px/MHz , respectively. As a first test, we mask a band of width 18.5 MHz (25 pixels) through the center of the burst and pass this zero-padded signal through our pipeline.

The fitting procedure on the 2D autocorrelation returns $a_{\text{fit}} = 102.7 \text{ pixels}$, $b_{\text{fit}} = 14.8 \text{ pixels}$, and $\theta_{\text{fit}} = 9.83^\circ$. The process is visualized in Figure 4. For such a small inclination angle, the percentage error in t_w is very close to that of b , and is (in this case) approximately 1%. The corresponding percentage error in the sub-burst drift dv_{obs}/dt_D is 1.7%.

We can generalize this test by shifting the frequency masking band of Figure 4 vertically. Upon doing so, we find that the error is independent of the frequency band's vertical position. The percentage error for the burst duration is found to be $\approx (-1.4 \pm 0.4)\%$, where the $\pm 0.4\%$ uncertainty applies to all band vertical positions tested, while the corresponding error in the angle is $\approx (-1.1 \pm 0.7)\%$.

If we rotate the burst of Figure 4, while retaining the central band mask of 18.5 MHz (25 pixels) on burst centre, we observe a linear enhancement of error with increasing orientation. The effect is, however, a negligible one: for every burst rotation by 10° , the duration error increases by only 0.45%, while the orientation angle error decreases (or increases in magnitude) by only 0.12° . At a 30.0° burst angle, the sub-burst drift error is only 4%.

3.3 The narrow-band nature of the emission process

As discussed in Section 1.1, data from Gajjar et al. (2018) and Hessels et al. (2019) is consistent with a rest frame frequency of 12102 Hz .

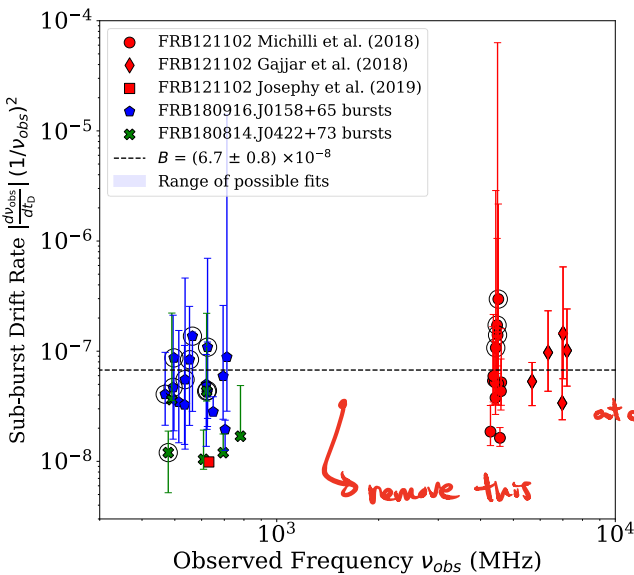


Figure 5. A plot of $(1/\nu_{\text{obs}}^2) |d\nu_{\text{obs}}/dt_0|^2$ vs. ν_{obs} for FRB 121102 (red circles, diamonds and square from Gajjar et al. 2018, Michilli et al. 2018 and Josephy et al. 2019, respectively), FRB 180916.J0158+65 (blue pentagons; CHIME/FRB et al. 2020) and FRB 180814.J0422+73 (green crosses; CHIME/FRB et al. 2019). The broken black line is for a fit to a constant B on the combined data for the three sources, with $B \equiv (\tau'_D \nu_0)^{-1} = (6.7 \pm 0.8) \times 10^{-8}$. The capped lines at each point represent the range of possible values due to the range of sub-drifts measured at different DMs, as discussed in Section 2.1. These are used in lieu of the unknown true measurement errors but are necessarily larger than the true errors. The shaded region indicates the range of possible fits for the constant B when accounting for the range of possible sub drift values and ranges from 2.1×10^{-8} to 3.5×10^{-6} .

emission ν_0 that does not change significantly from burst to burst. The results presented here further indicate a narrow-band emission process by inserting equation (2) into equation (1) to obtain

$$\frac{1}{\nu_{\text{obs}}^2} \frac{d\nu_{\text{obs}}}{dt_D} = -\frac{1}{\nu_0 \tau'_D}, \quad (8)$$

for the sub-burst drift (normalized to ν_{obs}^2), which is then predicted to be independent of ν_{obs} and scale inversely with ν_0 . Figure 5 shows the corresponding plot using the same data as in Figure 1. The broken black line is for a fit to a constant B on the combined data for the three sources, with $B \equiv (\tau'_D \nu_0)^{-1} = (6.7 \pm 0.8) \times 10^{-8}$. While there is some scatter in the data, the expected lack of dependency with ν_{obs} is observed. Any deviation can easily be accounted for with the uncertainty on the DMs. As was the case for the temporal narrowing and sad trombone effect discussed in Section 1.1 for FRB 121102, this behavior would be affected if ν_0 changed significantly in equation (8).

Taken together the verification of these three predictions provide strong evidence that the underlying physical process responsible for the emission of FRB signals in these repeating FRBs is narrow-band in nature.

Finally, we note that our discovery of a shared sub-burst drift law among these three sources suggests that this could be a universal property among repeating FRBs or at least a significant subclass of them. This not only motivates further searches but also provides a new tool to study and categorize FRBs based on their underlying physical mechanism.

~ Insert here

4 CONCLUSION

We demonstrate a method of studying the difficult-to-measure sub-drift rate in the context of DM variations from burst to burst and over time by adopting large ranges of possible DMs when measuring spectro-temporal properties of FRBs. This method reveals that even given a wide range of possible DMs for each burst from an FRB source, the sub-drift rate of an individual FRB is inversely proportional to its duration. Furthermore, for the three sources considered in this work, namely FRB 121102, FRB 180916.J0158+65 and FRB 180814.J0422+73, significant overlap between the inverse trends found is consistent with the three relationships having a nearly identical scaling. That is, the same law can be used to describe bursts from all three sources, though a more careful treatment of each burst's DM would be needed to prove this.

We believe that the simplest explanation for the existence of this trend is that the emission mechanism of these FRB sources is narrow-band in nature, and that if indeed multiple sources obey the same scaling of the law, then a single line transition may be responsible for the FRB phenomenon through, for example, Dicke's superradiance. Such a mechanism requires a trigger, which leaves room for magnetar-centric models of FRBs within the context of this result. To study this relationship further future analysis of FRBs from all known repeater sources can be performed to test the hypothesis that all FRB repeaters can be characterized by such an inverse law. A large sample of sources helps to constrain the error due to variations in DM, and necessitates convenient and public access to FRB data.

If deviations from this relationship exist, then it is likely the sub-drift law can serve as a classification tool for FRB sources by discriminating sources that follow this law from those that do not.

To further study the relationship between the sub-burst drift & temporal duration future ...

ACKNOWLEDGEMENTS

The authors are grateful to Z. Pleunis and S. Tendulkar from the CHIME/FRB Collaboration for their help in accessing and analyzing the data for FRB 180916.J0158+65 and FRB 180814.J0422+73. M.H. is grateful for the hospitality of Perimeter Institute where part of this work was carried out. M.H.'s research is funded through the Natural Sciences and Engineering Research Council of Canada Discovery Grant RGPIN-2016-04460. F.R.'s research at Perimeter Institute is supported in part by the Government of Canada through the Department of Innovation, Science and Economic Development Canada and by the Province of Ontario through the Ministry of Economic Development, Job Creation and Trade. F.R. is in part financially supported by the Institute for Quantum Computing. C.M.W. and A.M. are supported by the Natural Sciences and Engineering Research Council of Canada (NSERC) through the doctoral post-graduate scholarship (PGS D).

DATA AVAILABILITY

The data pipeline is made available at <https://github.com/mef51/subdriftlaw> and maintained by M.A.C. Aggregate data of the bursts and the code for the figures are also available. Data of the FRB spectra are available either publicly or via the authors of their respective publications. The figures in this paper were prepared using the `matplotlib` package (Hunter 2007).

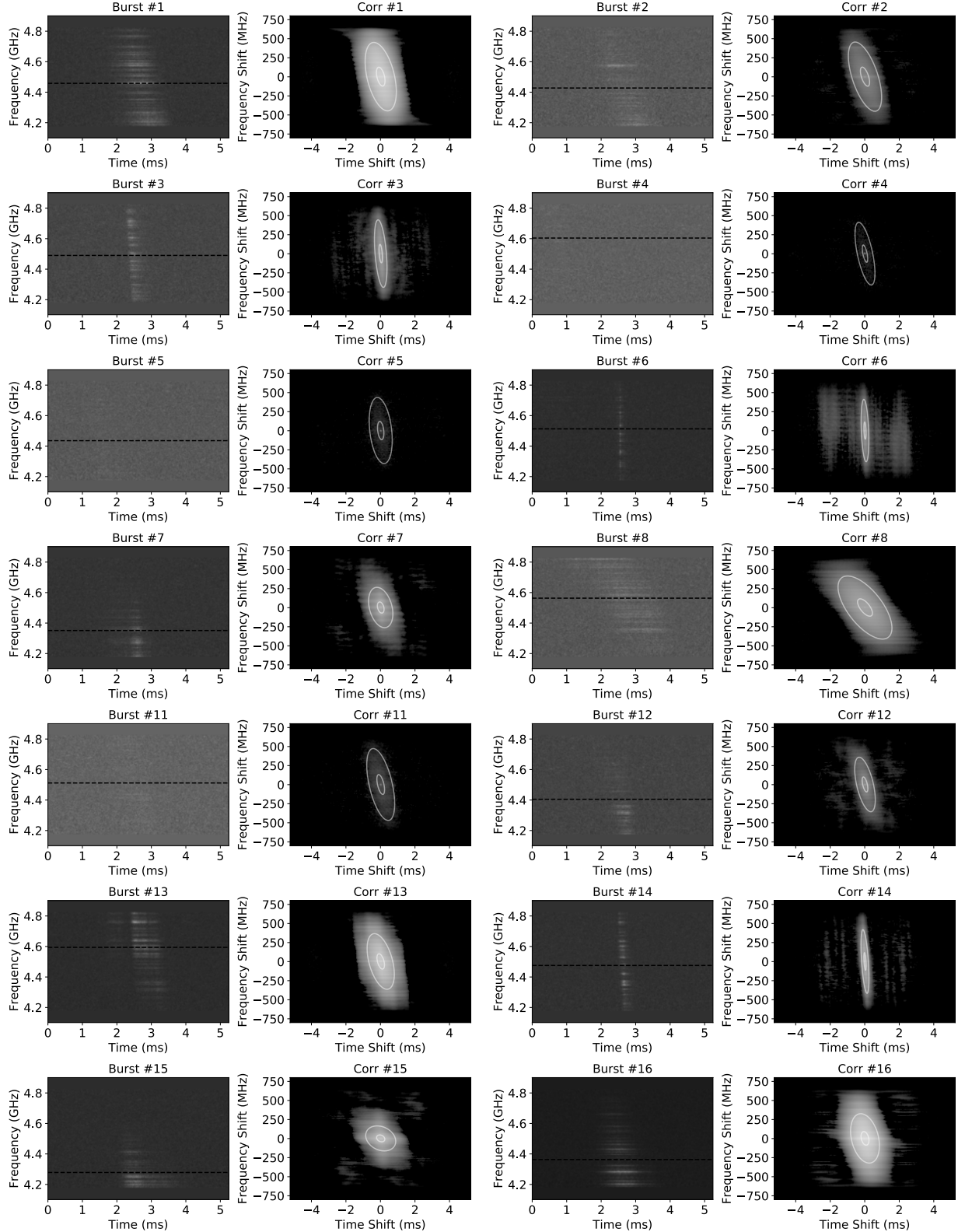


Figure 6. Dynamic spectra (first and third columns) and corresponding autocorrelation functions (second and fourth columns) for FRB 121102 bursts at a frequency of approximately 4–5 GHz from Michilli et al. (2018). The dynamic spectra were de-dispersed with a DM = 559.7 pc cm⁻³ and the dashed horizontal line in the dynamic spectra denotes the center frequency ν_{obs} used for the analysis. The autocorrelation functions are modelled with a 2D Gaussian ellipsoid whose one- and two-standard deviation levels are shown using the white contours.

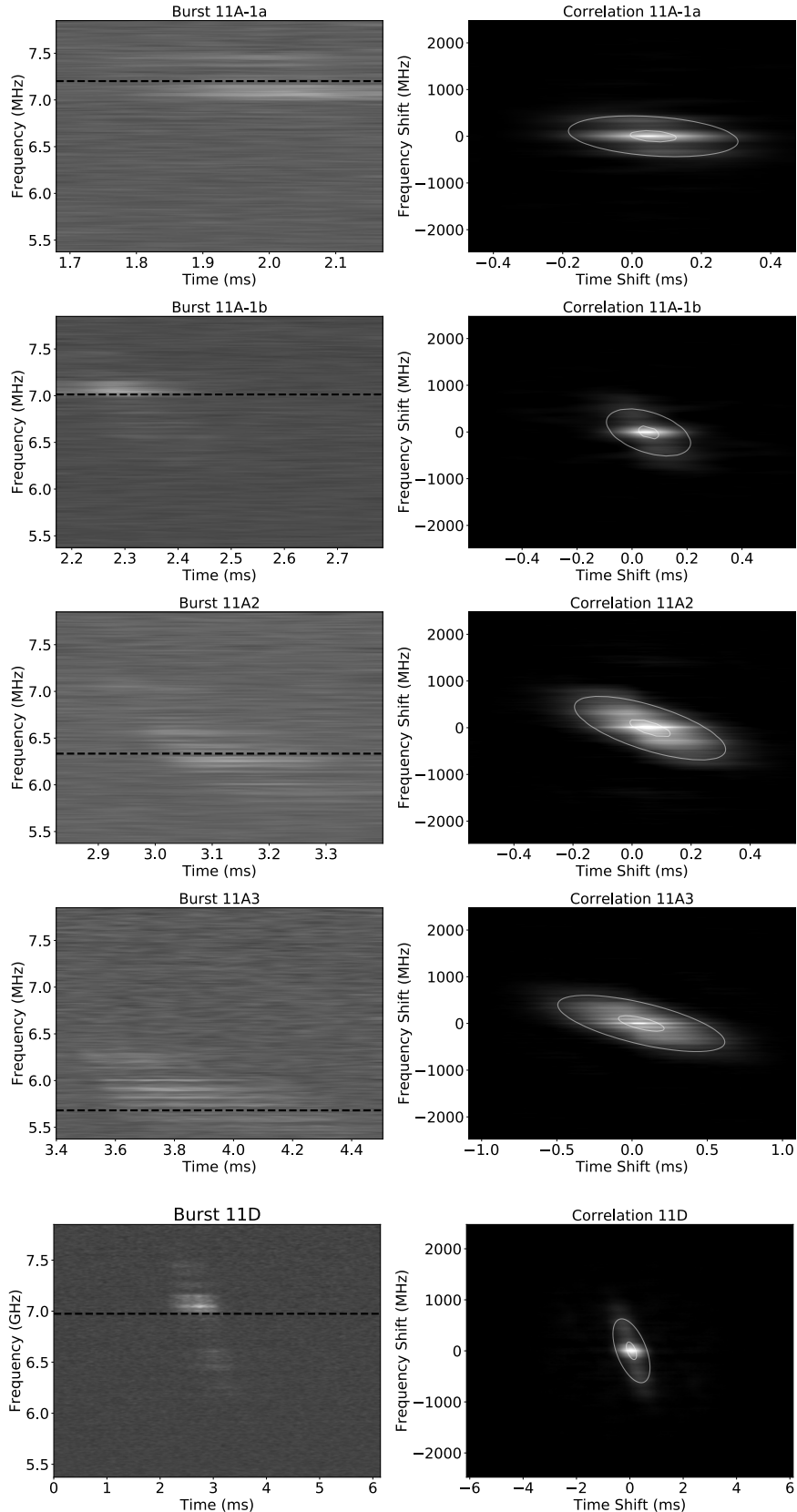


Figure 7. Same as Figure 6 but for the FRB 121102 data at approximately 5–8 GHz published in Gajjar et al. (2018) and de-dispersed with a DM = 565 pc cm⁻³. The top four sub-bursts are taken from one event, i.e., Burst 11A. Note that the time axes for the autocorrelation functions do not all share the same range, which distorts their relative appearance.

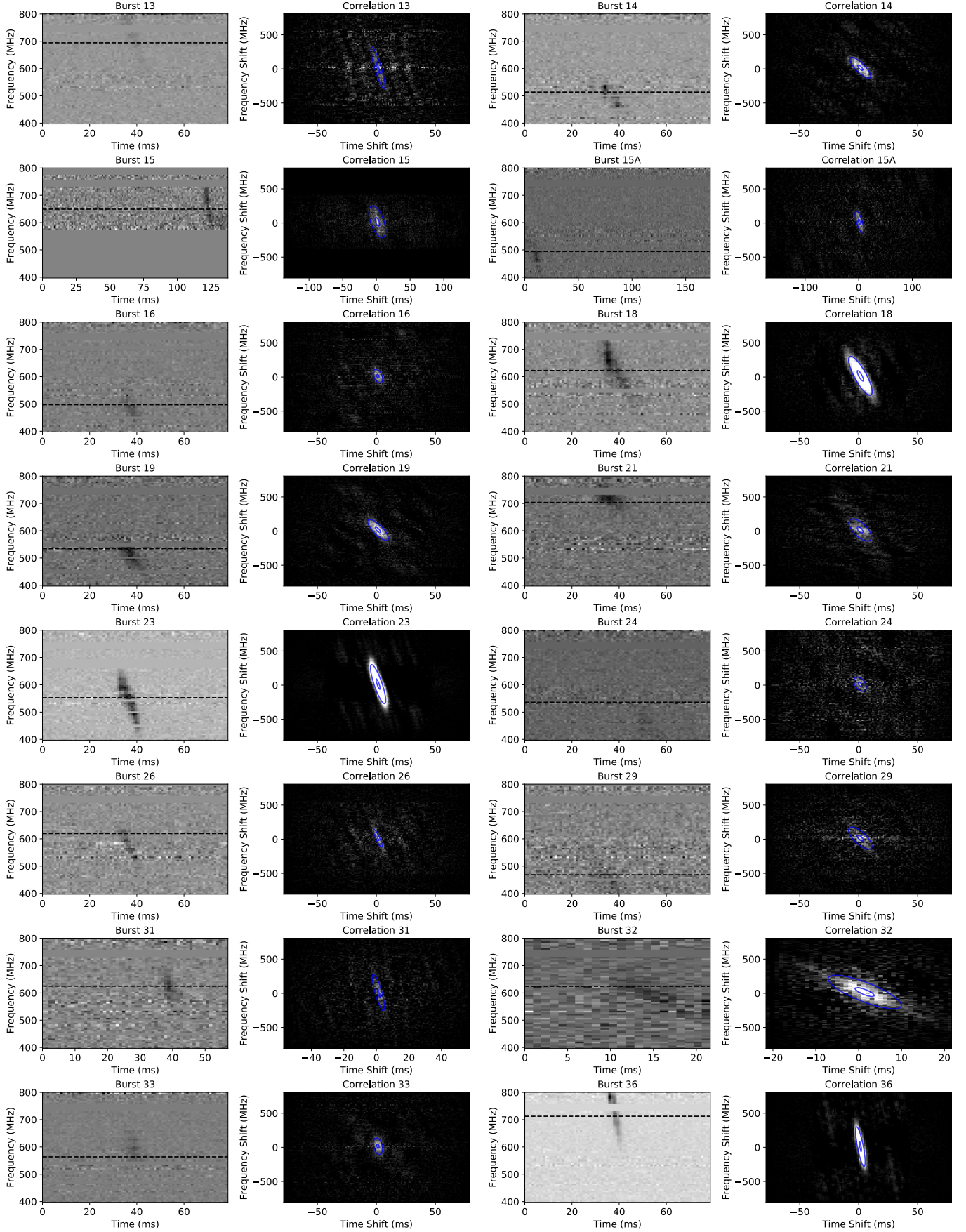


Figure 8. Same as Figure 6 but for FRB 180916.J0158+65 taken from CHIME/FRB et al. (2020). These data were de-dispersed with a DM = 348.82 pc cm⁻³. Note that the time axes for the autocorrelation functions do not all share the same range, which distorts their relative appearance.

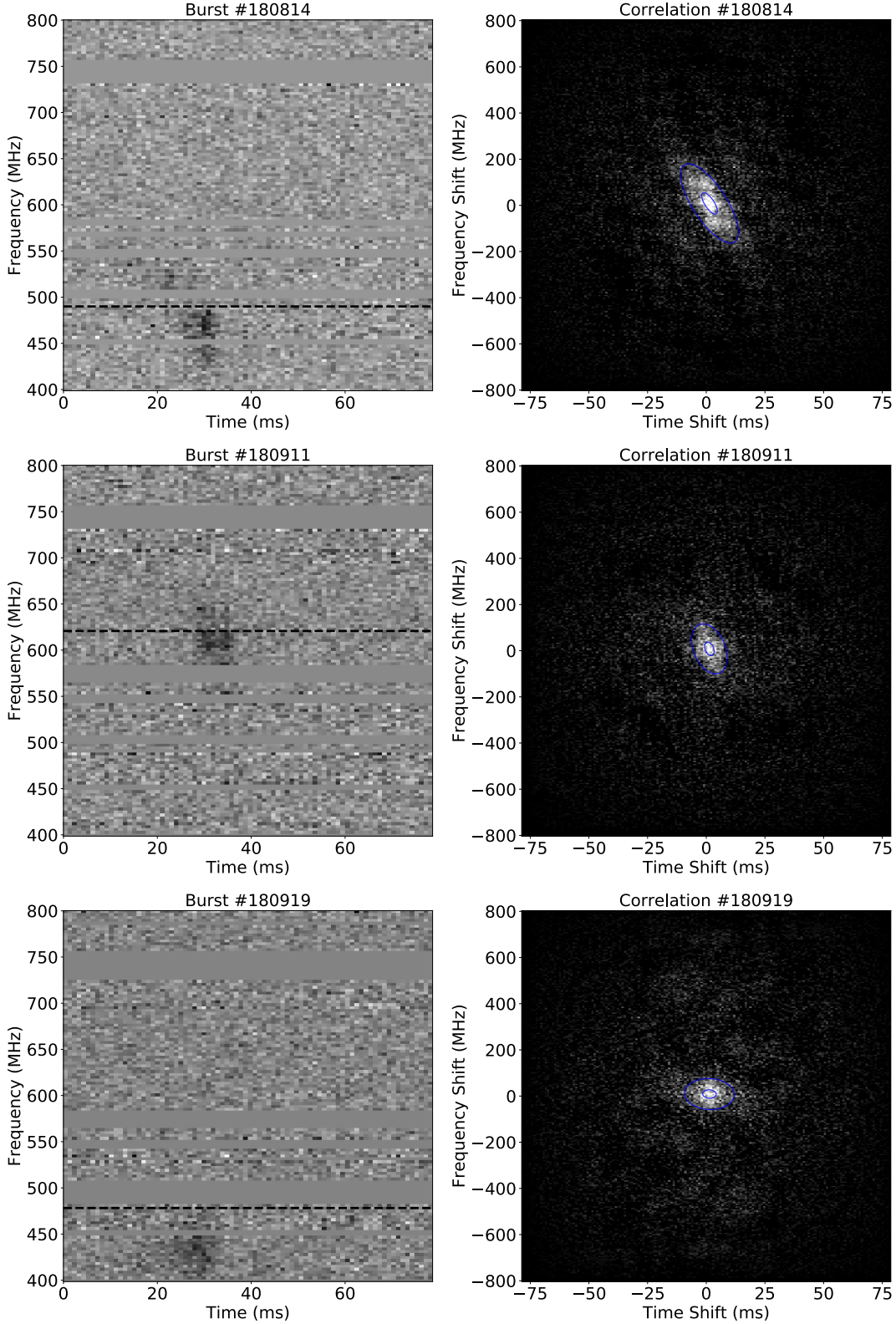


Figure 9. Same as Figure 6 but for FRB 180814.J0422+73 taken from CHIME/FRB et al. (2019). These data were de-dispersed with a $\text{DM} = 188.9 \text{ pc cm}^{-3}$.

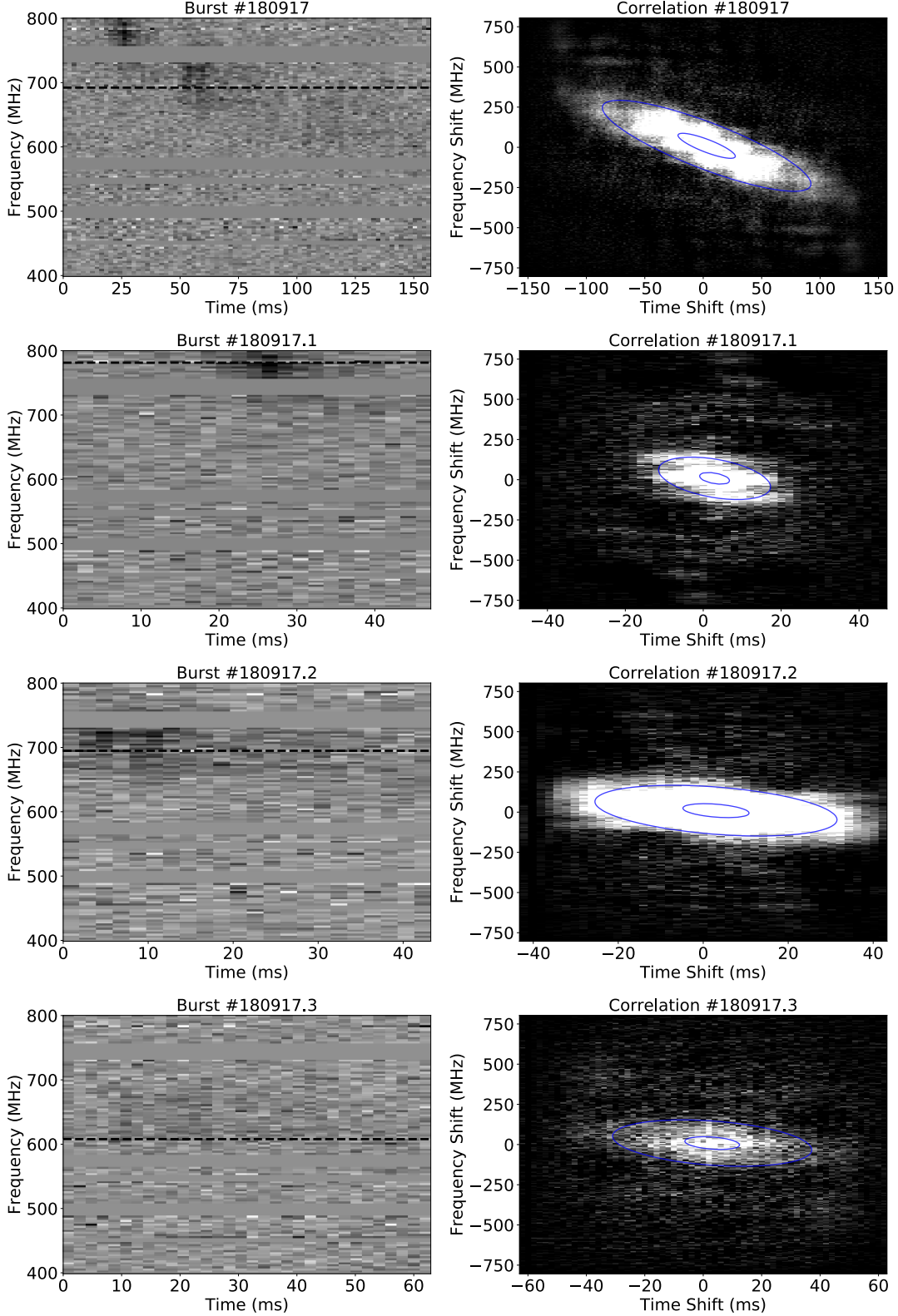


Figure 10. Same as Figure 9 but for Burst #180917 of FRB 180814.J0422+73 taken from CHIME/FRB et al. (2019). The whole event is shown on the top row (not used for Figure 1 of main text), while its three separate sub-bursts are detailed in the bottom three (all used for Figure 1 of main text). Note that the time axes for the autocorrelation functions do not all share the same range, which distorts their relative appearance.

REFERENCES

- Beloborodov A. M., 2020, *ApJ*, 896, 142
 Beniamini P., Kumar P., 2020, *MNRAS*, 498, 651
 Bochenek C. D., Ravi V., Belov K. V., Hallinan G., Kocz J., Kulkarni S. R.,
 McKenna D. L., 2020, *Nature*, 587, 59
 CHIME/FRB Collaboration Andersen B., et al., 2019, *ApJ*, 885, L24
 CHIME/FRB et al., 2019, *Nature*, 566, 235
 CHIME/FRB Amiri M., et al., 2020, *Nature*, 582, 351
 Cordes J. M., Wasserman I., Hessels J. W. T., Lazio T. J. W., Chatterjee S.,
 Wharton R. S., 2017, *ApJ*, 842, 35
 Fedorova V. A., Rodin A. E., 2019, *Astron. Rep.*, 63, 39
 Fonseca E., et al., 2020, *ApJ*, 891, L6
 Gajjar V., et al., 2018, *ApJ*, 863, 2
 Hessels J. W. T., et al., 2019, *ApJ*, 876, L23
 Houde M., Mathews A., Rajabi F., 2018, *MNRAS*, 475, 514
 Houde M., Rajabi F., Gaensler B. M., Mathews A., Tranchant V., 2019,
 MNRAS, 482, 5492
 Hunter J. D., 2007, *Computing in Science & Engineering*, 9, 90
 Josephy A., et al., 2019, *ApJ*, 882, L18
 Kirsten F., Snelders M. P., Jenkins M., Nimmo K., van den Eijnden J.,
 Hessels J. W. T., Gawroński M. P., Yang J., 2020, *Nature Astronomy*,
 Li Y., Zhang B., Nagamine K., Shi J., 2019, *ApJ*, 884, L26
 Lorimer D. R., Bailes M., McLaughlin M. A., Narkevic D. J., Crawford F.,
 2007, *Science*, 318, 777
 Marcote B., et al., 2020, *Nature*, 577, 190
 Mathews A., 2017, The Role of Superradiance in Cosmic Fast Radio Bursts,
 Honours thesis, The University of Western Ontario
 Metzger B. D., Margalit B., Sironi L., 2019, *MNRAS*, 485, 4091
 Michilli D., et al., 2018, *Nature*, 553, 182
 Petroff E., Hessels J., Lorimer D., 2019, *A&ARv*, 27, 4
 Pleunis Z., 2020, PhD thesis, McGill University
 Press W. H., Teukolsky S. A., Vetterling W. T., Flannery B. P., 2007, *Numerical Recipes* 3rd Edition: The Art of Scientific Computing, 3 edn.
 Cambridge University Press, USA
 Rajabi F., Houde M., 2016a, *ApJ*, 826, 216
 Rajabi F., Houde M., 2016b, *ApJ*, 828, 57
 Rajabi F., Houde M., 2017, *Sci. Adv.*, 3, e1601858
 Rajabi F., Houde M., 2020, *MNRAS*, 494, 5194
 Rajabi F., Houde M., Bartkiewicz A., Olech M., Szymczak M., Wolak P.,
 2019, *MNRAS*, 484, 1590
 Rajabi F., Chamma M. A., Wyenberg C. M., Mathews A., Houde M., 2020,
 MNRAS, 498, 4936
 Rajwade K., et al., 2020, *MNRAS*, 495, 3551
 Rybicki G. B., Lightman A. P., 1979, Radiative processes in astrophysics.
 New York: Wiley
 Simard D., Ravi V., 2020, *ApJ*, 899, L21
 Tendulkar S. P., et al., 2017, *ApJ*, 834, L7
 The CHIME/FRB Collaboration Andersen B. C., et al., 2020, *Nature*, 587,
 54
 Wang W., Zhang B., Chen X., Xu R., 2019, *ApJ*, 876, L15

APPENDIX A: AUTOCORRELATION ANALYSIS

We discuss here the process of preparing and obtaining measurements from the dynamic spectra of bursts, based on the autocorrelation technique described in [Hessels et al. \(2019\)](#).

As mentioned in Section 2.1 when a dynamic spectrum consists of a train of multiple sub-bursts we separate the components and measure the drift rate and duration of each sub-burst separately. The dynamic spectra of every burst used in this analysis with its autocorrelation is shown in Figures 6 – 10.

The pipeline that every sub-burst undergoes is written in Python and consists of computing the autocorrelation of the signal, fitting a two-dimensional (2D) Gaussian to the resulting autocorrelation function, and a calculation of the physical quanti-

ties of interest from the fit parameters: namely the sub-burst drift rate and duration. The autocorrelation of the dynamic spectrum measures the self-similarity of the sub-burst in frequency-time space and for FRBs can be approximated by an ellipsoid with an intensity that follows a 2D Gaussian ([Hessels et al. 2019](#)). Before computing the autocorrelation and depending on the source and/or burst, some noise removal is performed. For the bursts from FRB 121102 and FRB 180916.J0158+65 this is done by subtracting from the entire spectrum a background signal obtained from a time-average of twenty or so samples taken prior to the burst. For FRB 180814.J0422+73, due to the raw format the bursts are provided in, a noise mask was acquired through correspondence with members of the CHIME/FRB Collaboration and the channels are normalized by the standard deviation of the intensity. Missing or blocked out frequency channels in dynamic spectra (e.g., because of radio frequency interference (RFI)) are zeroed out before performing the autocorrelation.

The computation of the autocorrelation function is facilitated and sped up by using a Fast Fourier Transform (FFT) of the dynamic spectrum, which is then squared and inverted (through an FFT) back to the frequency-time domain ([Press et al. 2007](#)). The autocorrelation function is then modelled with the following functional form for a rotated 2D Gaussian

$$G(x, y) = C \exp \left\{ -\frac{1}{2} \left[x^2 \left(\frac{\cos^2 \theta}{b^2} + \frac{\sin^2 \theta}{a^2} \right) + 2xy \sin \theta \cos \theta \left(\frac{1}{b^2} - \frac{1}{a^2} \right) + y^2 \left(\frac{\sin^2 \theta}{b^2} + \frac{\cos^2 \theta}{a^2} \right) \right] \right\}, \quad (\text{A1})$$

with the free parameters C , a , b , and θ for, respectively, the amplitude, the semi-major and semi-minor axes (i.e., the standard deviations) of the ellipsoid, and the sub-drift angle for the orientation of the semi-major axis measured counterclockwise from the positive y -axis. More precisely, the x - (i.e., for the time lag) and y -axes (i.e., for the frequency lag) are respectively oriented horizontally and vertically on the autocorrelation plots shown in Figures 6–10. To find these parameters we use the `scipy.optimize.curve_fit` package, which performs a non-linear least squares fit. The package also returns a covariance matrix, which is used to calculate the uncertainty of the fitted parameters. These uncertainties are then scaled by the square-root of the reduced χ^2 computed from the residual between the autocorrelation function and its Gaussian fit. We note again that the uncertainty calculated this way does not capture nearly the entire error budget which depends more significantly on the error in the DM ([discussed in Section 2.1](#)) as well the parts of the burst spectra that have been masked out and the shape of its autocorrelation. → [ref to see 3.2](#)

Using the angle θ , the sub-burst drift rate is calculated via

$$\frac{d\nu_{\text{obs}}}{dt_D} = -\frac{\nu_{\text{res}}}{t_{\text{res}}} \cot \theta, \quad (\text{A2})$$

where ν_{res} and t_{res} are the frequency and time resolutions of the dynamic spectrum. We obtain the sub-burst duration from the fit parameters through

$$t_w = t_{\text{res}} \frac{ab}{\sqrt{b^2 \sin^2 \theta + a^2 \cos^2 \theta}}. \quad (\text{A3})$$

These expressions are also used to propagate the fit parameter uncertainties to the values of $d\nu_{\text{obs}}/dt_D$ and t_w . These uncertainties are used to confirm the claim that DM variations are the largest source of error, as stated in Section 2.1.

The observation frequency ν_{obs} of each burst is estimated via an intensity-weighted average of the spectrum over the whole time range. While this decreases the accuracy of the estimate as opposed to using just the on-pulse region, we find it has little bearing on the result. To fit equation (1) we used the `scipy.odr.RealData` package, which uses orthogonal distance regression and uses the uncertainties on the data to find a fit. We use the range of measurements obtained over the range of trial DMs as the uncertainty when performing this fit. → I don't think so...

APPENDIX B: DETERMINATION OF β^+ , ν_0 AND $\Delta\beta'$

The equations presented in this section apply to cases where the source of radiation travels directly toward or away from the observer.

For the determination of the maximum speed of an FRB rest frame toward the observer $\beta^+ > 0$ and ν_0 , the frequency of emission within it, we can generally set $\beta^- = -a\beta^+$ with $a \geq 0$ for the greatest (i.e., most negative) speed away from the observer. Using the relativistic Doppler shift formula (Rybicki & Lightman 1979) for the corresponding frequencies in the observer's rest frame

$$\nu_{\text{obs}}^\pm = \nu_0 \sqrt{\frac{1 + \beta^\pm}{1 - \beta^\pm}}, \quad (\text{B1})$$

we find that

$$\begin{aligned} \beta^+ &= \left(\frac{1+a}{2a} \right) \left(\frac{\nu_{\text{obs}}^+{}^2 + \nu_{\text{obs}}^-{}^2}{\nu_{\text{obs}}^+{}^2 - \nu_{\text{obs}}^-{}^2} \right) \\ &\times \left[1 - \sqrt{1 - \frac{4a}{(1+a)^2} \left(\frac{\nu_{\text{obs}}^+{}^2 - \nu_{\text{obs}}^-{}^2}{\nu_{\text{obs}}^+{}^2 + \nu_{\text{obs}}^-{}^2} \right)^2} \right] \end{aligned} \quad (\text{B2})$$

$$\nu_0^2 = \nu_{\text{obs}}^+ \nu_{\text{obs}}^- \sqrt{\frac{1 - (1-a)\beta^+ - a\beta^{+2}}{1 + (1-a)\beta^+ - a\beta^{+2}}}. \quad (\text{B3})$$

The discussion in Section 3 where the FRB rest frames span the range $\pm\beta^+$ corresponds to the case $a = 1$, which reduces equations (B2)-(B3) to equations (4)-(5) of the main text. We also note that a system becomes most strongly relativistic when $a \rightarrow 0$ where $\nu_0 \rightarrow \nu_{\text{obs}}^-$, while the opposite is true as $a \rightarrow \infty$ and $\nu_0 \rightarrow \nu_{\text{obs}}^+$.

For the determination of $\Delta\beta'$, we start by considering that for a signal initially observed at frequency ν_{obs} a velocity change $\Delta\beta$ in the observer's rest frame will be accompanied by a change $\delta\nu_{\text{obs}}$ in frequency given by

$$\frac{\delta\nu_{\text{obs}}}{\nu_{\text{obs}}} = \frac{\Delta\beta}{1 - \beta^2}, \quad (\text{B4})$$

where β is the initial velocity relative to the observer. Using the special relativistic velocity addition law (Rybicki & Lightman 1979) we can relate the velocity changes in the observer and FRB rest frames through

$$\Delta\beta = \Delta\beta' \left(\frac{1 - \beta^2}{1 + \beta\Delta\beta'} \right), \quad (\text{B5})$$

with $\Delta\beta'$ the corresponding velocity change in the FRB frame.

Allowing for the motions within the FRB rest frame to span the range $\pm\Delta\beta'$ (with $\Delta\beta' \geq 0$; for simplicity, we assume a symmetric velocity range about zero), while using equations (B1) (to express β as a function of ν_{obs} and ν_0) and (B4)-(B5), we find the following relation for the total observed bandwidth covered by the

corresponding signals

$$\frac{\Delta\nu_{\text{obs}}}{\nu_{\text{obs}}} = 2\Delta\beta' \left[1 - \Delta\beta'^2 \left(\frac{\nu_{\text{obs}}^2 - \nu_0^2}{\nu_{\text{obs}}^2 + \nu_0^2} \right)^2 \right]^{-1}. \quad (\text{B6})$$

Equation (6) follows from this relation, which reaches a maximum value when $\nu_{\text{obs}} = 0$ or $\nu_{\text{obs}} \gg \nu_0$. While equation (B6) shows little variations whenever $\Delta\beta' \ll 1$, it could, in principle, be used to evaluate the FRB rest frame frequency ν_0 independently of equation (B3) since it reaches a minimum of $2\Delta\beta'$ at $\nu_{\text{obs}} = \nu_0$. However, the effect is probably too small (on the order of 1% for FRB 121102) to be measurable given the scatter inherent to FRB data.

This paper has been typeset from a `TeX/LaTeX` file prepared by the author.